NUMERICAL PREDICTION OF VERTICAL SHIP MOTIONS AND ADDED RESISTANCE

(DOI No: 10.3940/rina.ijme.2017.a4.450)

F Cakici, **E Kahramanoglu**, and **A D Alkan**, Yildiz Technical University, Turkey

SUMMARY

Along with the development of computer technology, the capability of Computational Fluid Dynamics (CFD) to conduct 'virtual computer experiments' has increased. CFD tools have become the most important tools for researchers to deal with several complex problems. In this study, the viscous approach called URANS (Unsteady Reynolds Averaged Navier-Stokes) which has a fully non-linear base has been used to solve the vertical ship motions and added resistance problems in head waves. In the solution strategy, the FVM (Finite Volume Method) is used that enables numerical discretization. The ship model DTMB 5512 has been chosen for a series of computational studies at Fn=0.41 representing a high speed case. Firstly, by using CFD tools the TF (Transfer Function) graphs for the coupled heave-pitch motions in deep water have been generated and then comparisons have been made with IIHR (Iowa Institute of Hydraulic Research) experimental results and ordinary strip theory outputs. In the latter step, TF graphs of added resistance for deep water have been generated by using CFD and comparisons have been made only with strip theory.

NOMENCLATURE

A	Wave amplitude (m)
B_{WL}	Waterline breadth (m)
C_{AW}	Added resistance coefficient (-)
Cb	Block coefficient (-)
Cm	Midship section coefficient (-)
f	Wave frequency (s^{-1})
fe	Encounter wave frequency (s^{-1})
Fn	Froude number (-)
g	Gravitational acceleration ($m\ s^{-2}$)
Iy	Inertia moment of mass ($kg\ m^2$)
k	Wave number (m^{-1})
LCG	Longitudinal position of center of gravity (m)
L_{PP}	Length between perpendiculars (m)
L_{WL}	Waterline length (m)
M	Mass (kg)
N	Number of elements (-)
r	Refinement factor (-)
R	Convergence coefficient (-)
R_{AW}	Added resistance (N)
R_F	Frictional resistance (N)
R_R	Residuary resistance (N)
R_T	Total resistance (N)
Re	Reynolds number (-)
S	Wetted surface area (m^2)
T	Draught (m)
T_e	Wave encounter period (s)
V	Ship speed (m/s)
VCG	Vertical position of center of gravity (m)
λ	Wave length (m)
CFD	Computational fluid dynamics
DFBI	Dynamic fluid body interaction
EEDI	Energy efficiency design index
GCI	Grid convergence index
IMO	Intergovernmental Maritime Organization
N-S	Navier-Stokes
FS	Fourier series
FVM	Finite volume method
TF	Transfer function
URANS	Unsteady Reynolds averaged Navier-Stokes
SMP	Ship Motion Program

1. INTRODUCTION

Ship motion computations even in regular waves are still one of the leading and challenging working areas for researchers. Difficulties mainly stem from the sources listed below:

- The second order velocity term when calculating the pressure acting on the hull surface.
- Flows are highly nonlinear around the ship and the Reynolds numbers covered in ship motions are usually high.
- In reality, waves are not in a simple sinusoidal form due to gravitational force.
- The complex ship geometries majorly affect the restoring terms in the equations of ship motions.
- Kelvin wave pattern of the ship in given advancing velocity may affect the ship motions in waves especially at high Froude numbers.

In addition to these, performing seakeeping tests are difficult and costly compared with experiments dealing with the resistance characteristics for displacement types of models. The primary reason is that measured forces and moments are strongly time-dependent in seakeeping tests compared with a fixed hull in resistance experiments. Some additional difficulties include:

- Measuring the amplitude of the waves reaching the ship. Also, the amplitudes of the generated waves tend to change until the ship encounters them.
- Determination of the radius of inertia of the ship with a sufficient level of accuracy is difficult.

Therefore, developing numerical methods may support experiments by using their flow visualization abilities or in some cases they may even be used as a substitute for experiments due to the above-mentioned difficulties in ship motion experiments. In fact, ship motion experiments are generally used to validate numerical approaches in the academic world (Bertram, 2000).

As a numerical approach, URANS and the additional turbulence equations, which are discretized by using FVM, have recently been implemented to obtain vertical ship motions and added resistance in waves. However, some potential methods for vertical ship motions and added resistance calculations in deep water have been used, as mentioned in a comprehensive study of Tezdogan et al. (2015) and related references reported therein.

In this section, pioneering studies associated with URANS are given. Sato et al. (1999) studied the coupled vertical motions for Wigley and Series 60 hull forms at head waves. They compared their results with experimental data and concluded that CFD analyses are in good accordance with experiments for the Wigley hull but not for the Series 60 hull form. Beck and Reed (2001) advised that the best options to solve maritime problems are 3D URANS methods. Carrica et al. (2006) studied the forward speed diffraction problem for the DTMB 5512 model under head seas at two speeds and two wavelengths. They discovered that relatively short wavelength waves show non-linear characteristics on heave forces and pitch moments with a remarkable second harmonic component. In their following study, for the same ship model, Carrica et al. (2007) performed URANS analyses to compute the heave and pitch motions in small and large amplitude regular head waves for near-resonant cases. They observed transom wave breaks and extreme motions in large amplitude cases. They only dealt with the encounter frequency near the resonance region. Irvine et al. (2008) carried out seakeeping towing tank experiments of coupled pitch and heave motions and presented a very large database for vertical motions for DTMB 5512. Weymouth et al. (2005) also carried out seakeeping simulations by implementing CFD. Their results were compatible with experiments and they advised possible methods to be implemented in a wide Froude number range. However, in this study the motions were investigated only for a low wave slope range. High wave slope ranges were investigated by Deng et al. (2009) and they studied the vertical motions of a benchmark container ship form. However, in their study, differences for added resistance calculations were quite high compared with experiments. Wilson et al. (2008) performed CFD analyses to obtain TF's of vertical responses of the S-175 ship in regular head waves. The nonlinear URANS approach was used by many researchers to find the hydrodynamic coefficients regarding the added mass as well as the damping. One of these studies was the work of Querard et al. (2009) and they dealt with the computations of added mass and damping of 2D sections. Calculations were done for a very wide range of frequency spectrum. The main focus of their work was to make a comparison with the results obtained by the potential theory; therefore, the motions of the sections that they selected were rather low. For this reason, Querard's method is more accurate compared with potential methods but still deficient due to low motion amplitude. Bhushan et al. (2009) carried out vertical ship motion analyses for both the model and the full scale of the Athena hull form. Simonsen et al. (2010 and 2013) prepared a comprehensive study by using CFD for many different types of ships for seakeeping calculations. Guo et al. (2012) investigated the vertical motions for head waves of the KVLCC2 hull model by using URANS and made added resistance predictions. They showed that CFD can be used for vertical motions and added resistance calculations by comparing the results with experimental data. Tezdogan et al. (2015) investigated the behaviour of vertical motions and added resistance in waves for the full scale KRISO Container model. Their predictions were quite satisfactory. Ozdemir and Barlas (2017) focused on resistance in calm water, ship motions and added resistance calculations for the KVLCC2 model. They claimed that their numerical prediction was in good agreement for resistance, pitch and heave motions. However, an accurate prediction was not achieved for added resistance calculations.

In this study, the TF graphs for the coupled pitch and heave motions in regular head waves were obtained by using CFD for regular frequencies which were the same as those in the experiments conducted in IIHR (Irvine et al., 2008). Added resistance calculations were also performed for the same scenario. Both calculations were carried out in the deep water case for Fn=0.41. While CFD vertical motion TF graphs were compared with experiment and strip theory, CFD added resistance TF graphs were only compared with strip theory. The papers of Salvesen et al. (1970) and Salvesen (1978) was used for comparison of vertical ship motions and added resistance in waves with CFD. The resistance characteristics of the ship in calm water were also calculated for the purpose of validation as shown in Section 5. The commercial CFD software Star-CCM+ was used to discretize the URANS equations by implementing FVM.

This study has two main aims:

1. To compare two numerical techniques and take advantage of their benefits when obtaining vertical motions in head waves for a high speed case. In addition to Carrica's work (2006 and 2007), in the present study, the performed analysis covers the whole frequency range for validation with the experiment.
2. To compare the CFD added resistance TF graph in regular waves against strip theory for a high speed case.

This paper is organised as follows. In Section 2, the main dimensions and physical conditions are presented. In Section 3, the governing equations with computational domain, time step selection, mesh generation and Fourier Series formulation for the problem are given. CFD verification and validation studies are presented in Section 4. Finally, results and discussions are given in Section 5.

 ©2017: The Royal Institution of Naval Architects

The reader should be reminded that experimental results are not available for the second purpose.

2. MAIN PARTICULARS AND PHYSICAL CONDITIONS

A 1/46.588 scaled model of the DTMB 5512 hull given in Figure 1 was used. The experimental results are given in the paper of Irvine et al. (2008). The geometric feature of the model hull is given in Table 1. The numerical simulations were carried out for the bare hull only.

Table 1: Geometric feature of the model

Main Parameters	Value
L_{PP}	3.048 m
L_{WL}	3.052 m
B_{WL}	0.409 m
T	0.132 m
M	84.2 kg
LCG (from aft)	1.536 m
VCG (from base line)	0.152 m
C_m	0.821
C_b	0.507
I_y	48.90 kg-m^2
V	2.2419 m/s
Fn	0.41

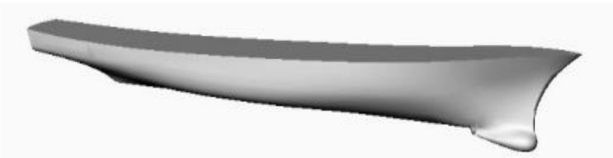

Figure 1: 3D representation of the DTMB 5512 model

An Earth-fixed Cartesian coordinate system xyz was selected for the solution domain. The xy plane represented the calm free water surface and z was defined as the vertical axis. The model was allowed to advance in the positive x direction with 2DOF vertical pitch and heave motions. A new local coordinate system was created for the ship to obtain 2DOF motion. The CFD and strip theory calculations were performed at seven different encounter frequencies for Fn=0.41 as shown in Table 2. All calculations were performed in deep water at regular head waves.

Wave encounter frequency can be defined as:

$$f_e = f + (\frac{2\pi f^2 V}{g}) \tag{1}$$

for the ship advancing in head seas. In Equation (1), g denotes the gravity, f denotes the frequency of the wave and V denotes the velocity of the ship. Small amplitude waves (Ak=0.025) were chosen for CFD simulations to be consistent with performed experiments by Irvine et al. (2008) where A denotes the wave amplitude and k denotes the wave number.

Table 2: Definition of cases for strip theory and CFD calculations

Case No	Method	Ak (-)	f_e (1/s)	A (m)	λ/L_{PP} (-)
1	CFD and Strip Theory	0.025	1.9918	0.0080	0.66
2			1.7388	0.0096	0.79
3			1.4572	0.0121	1.00
4			1.3032	0.0141	1.16
5			1.1448	0.0167	1.38
6			1.0766	0.0182	1.50
7			0.7972	0.0279	2.30

3. URANS EQUATIONS AND MODELLING

The averaged continuity and momentum equations can be written for incompressible flow in Cartesian coordinates and tensor form as indicated in Equations (2) and (3):

$$\frac{\delta U_i}{\delta x_i} = 0 \tag{2}$$

$$\rho(\frac{\delta U_i}{\delta t} + U_j \frac{\delta U_i}{\delta x_j}) = -\frac{\delta P}{\delta x_i} + \frac{\delta \tau}{\delta x_j} - \frac{\delta(\rho \overline{u_i' u_j'})}{\delta x_j} + F_i \tag{3}$$

where τ_{ij} are the mean viscous stress tensor components as shown in Equation (4).

$$\tau = \tau_{ij} = \mu(\frac{\delta U_i}{\delta x_j} + \frac{\delta U_i}{\delta x_i}) \tag{4}$$

In this paper, the two equation *k-ε* turbulence model was used to include the effects of the viscosity, as it is considered to be one of the most commonly used turbulence models for industrial applications (Querard, 2008). It is also cheaper in terms of computer memory compared to the k-*ω* SST model which requires higher CPU time (Tezdogan, 2016 and Querard, 2008). The employed solver uses a finite volume method which discretizes the Navier–Stokes (N-S) equations for the numerical model of fluid flow. Segregated flow model was used in the URANS solver, and convection terms in the URANS equations were discretized by applying a second order upwind scheme. In the analyses, the URANS solver runs a predictor–corrector SIMPLE-type algorithm between the continuity and momentum equations. A first-order temporal scheme was applied to discretize the unsteady term in the N-S equations. Volume of Fluid (VOF) model was used to represent the free surface. In this model, computations were performed for water and air phases. Due to the mesh structure and the number of elements having great importance in capturing the free surface deformations, some refinements were defined close to the free surface to accurately predict VOF wave profiles. A second order convection scheme was used to present the results calculated by VOF more precisely. Summary of the numerical discretization is given in Table 3.

Table 3: Numerical modelling properties

Temporal Discretization	First Order
Convection Term	Second Order
Pressure Link	SIMPLE
Turbulence Model	k- ε
VOF Wave	Second Order

The flow within the boundary layer has to be solved correctly for accurate calculation of the boundary layer dynamics. Therefore, y^+ values on the hull surface should remain within the limits for the *k-ε* turbulence model. The y^+ values on the hull surface were around 45 and this value is considered to be suitable since it remains between the recommended ranges 30-300 for the selected turbulence model (CD-Adapco, 2014). Two layer all y+ wall treatment was used.

The DFBI (Dynamic Fluid Body Interaction) module in the software STAR CCM+ was used for the motion of the body, and the vessel is set free to pitch and heave motions. The 2DOF motion of the body was obtained by calculating the velocity and pressure field in the fluid domain.

3.1 TIME STEP SIZE DETERMINATION

An explicit method generally requires a higher computer memory because of the relatively larger computational domain. In the explicit method, the CFL condition has to be satisfied for the stability of the method. In the present study, an implicit method was used due to computational limitations. In unsteady implicit problems, the restriction imposed by the CFL condition is not a strict issue anymore which frees up the computer in terms of required memory.

Time step size was selected to be $1/2^8$ of T_e for seakeeping analyses which is considered to be more accurate than the value recommended by ITTC (2011). Here T_e denotes the encounter period. The variation of time step size and the obtained results are given in the CFD verification and validation section.

3.2 COMPUTATIONAL DOMAIN AND BOUNDARY CONDITIONS

The given boundary and initial conditions must be proper for all analytical and numerical solutions to have a well-posed problem. These conditions must be determined according to the flow characteristics. In this study, the computational domain was created in order to simulate the seakeeping and added resistance behaviour of DTMB 5512 in regular waves for deep water.

Only half of the body was modelled in order to reduce the domain size and computational time. The boundary conditions for deep water cases are shown in Figure 2.

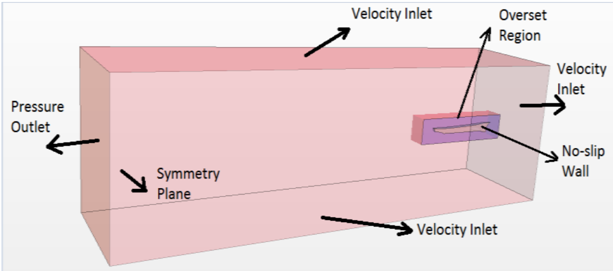

Figure 2: Boundary conditions of computational domain

The top, bottom and side boundaries were modeled as velocity inlet to avoid formation of boundary layers that would form near these boundaries as can be seen in Figure 2. By doing this, numerical simulation is accelerated. 5th-order Stokes waves were used to represent the regular wave for all CFD cases. This wave profile was selected because it is more similar to real waves than the one generated by the first order method (Fenton, 1985). The waves generated by advancing ship were dealt by implementing a numerical damping, which length is 0.50xLPP from the boundaries. A damping function was applied according to the study of Choi and Sung (2009).

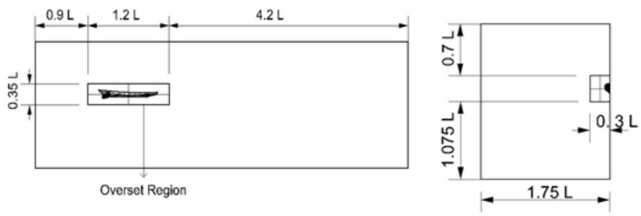

Figure 3: Sizes of the computational domain

As can be seen in Figure 3, the computational domain for deep water cases extended 0.9L in front of the overset region, 4.2L behind the overset region, and 1.75L to the side of the boundaries of the overset region and 1.075L under the boundaries of the overset region. The air region was 0.7L above the overset region.

3.3 MESH GENERATION

Overset mesh, which is considered to have great flexibility for bodies moving inside a fluid, was used for all calculations. This grid system, which is embedded in the background mesh enclosing a certain zone of domain, was used to represent the motion of the hull and there is an "overlap" zone that encompasses the overset region. The information is passed through the overlap block between the

©2017: The Royal Institution of Naval Architects

overset and background regions by using linear interpolation method. With the overset grid system, any mesh modification or deformation is not necessary which provides greater flexibility over other standard meshing techniques. In related references, overset mesh technique was used to represent vertical motions of the ships (Tezdogan et al., 2015), (Carrica et al., 2007).

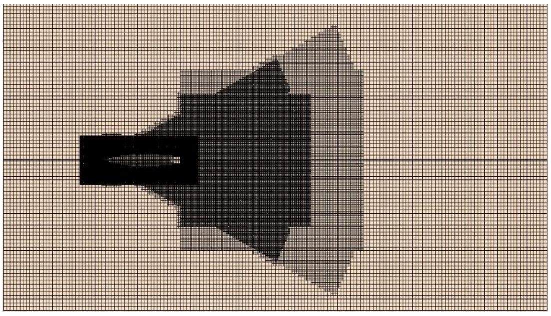
Figure 4: Mesh structure in free surface plane

The mesh was then refined at five regions; overset region, overlap region, vicinity of the hull, around free surface and Kelvin wake region where wave deformation is significant. Refinement blocks were also added near the ship's bow and stern regions in order to capture the pitch motion accurately. Figure 4 and Figure 5 show the mesh system in the computational domain for the deep water cases.

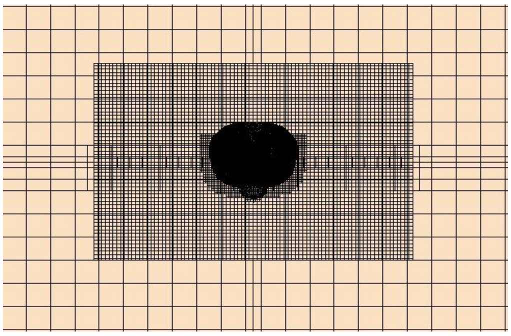
Figure 5a: Overset and overlap mesh structures around the ship

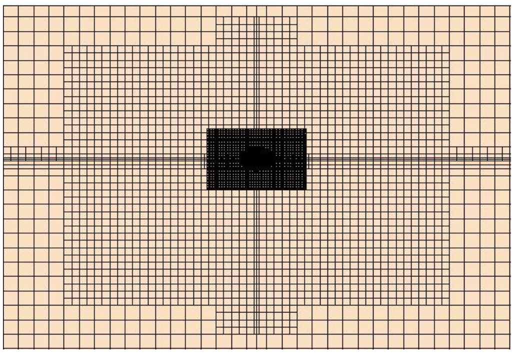
Figure 5b: Overall mesh structure in computational domain

Three different unstructured hexahedral mesh systems were used to calculate the numerical uncertainties which are coarse, medium and fine. The number of elements is given in Table 4. It has to be noted that the reference mesh is fine mesh.

Table 4: Number of elements

	Coarse Mesh	Medium Mesh	Fine Mesh
Background	2.24×10^5	2.24×10^5	2.24×10^5
Overset	3.40×10^5	4.83×10^5	7.25×10^5
Total	5.64×10^5	7.07×10^5	9.49×10^5

3.4 FOURIER SERIES (FS) EXPANSION

The FS formulation part is probably the most cumbersome part of the process because of the number of analyses. Unsteady time histories of the analyzed motions, $\eta(t)$ can be represented by using FS as indicated in Equation (5).

$$\eta(t) = \eta_0 + \sum_{n=1}^{N} \eta_n \cos(\omega_e t + \beta_n) \qquad n = 1,2,3... \tag{5}$$

In Equations (8) and (9), η_n and β_n denote the η_{th} harmonic amplitude and phase angle, respectively. These values can be calculated by using a_n and b_n in Equations (11) and (12) as follows.

η_0 is the zeroth harmonic of the unsteady signal which means the averaged value of the signal and it can be found by solving the integral given in Equation (8). η_0 can be used to obtain the added resistance in waves or resistance in calm water.

$$\eta_0 = \frac{1}{T_e} \int_0^{T_e} \eta(t) dt \tag{6}$$

$$\eta_n = \sqrt{a_n^{\ 2} + b_n^{\ 2}} \tag{7}$$

$$\beta_n = \arctan\left(\frac{b_n}{a_n}\right) \tag{8}$$

$$a_n = \frac{2}{T_e} \int_0^{T_e} \eta(t) \cos(2\pi f_e n t) dt \tag{9}$$

$$b_n = \frac{2}{T_e} \int_0^{T_e} \eta(t) \sin(2\pi f_e n t) dt \tag{10}$$

In these equations, T_e refers to the sampling time and is the encounter period of the given signal. Vertical ship motions, pitch and heave in regular waves can be expressed in terms of transfer functions by the following first harmonic statements given in Equations (11) and (12):

$$TF_{Heave} = \frac{\eta_{1Heave}}{A} \tag{11}$$

$$TF_{Pitch} = \frac{\eta_{1Pitch}}{Ak} \tag{12}$$

where A denotes the wave amplitude and k denotes the wave number.

4. CFD VERIFICATION AND VALIDATION

In the present study, uncertainty analysis was made by using the Grid Convergence Method. This method was first proposed by Roache (1998) and then applied in several studies with some improvements. Out of these refinements, in the present study, the procedure of Celik et al. (2008) has been implemented and is explained in this section.

The following method can be generally considered for unstructured mesh. The refinement factors r_{21} and r_{32} have been calculated according to Equation (13) by taking into account the number of cells.

$$r_{21} = \left(\frac{N_1}{N_2}\right)^{1/3} \qquad r_{32} = \left(\frac{N_2}{N_3}\right)^{1/3} \tag{13}$$

Heave motion numerical uncertainties have been investigated for Case no. 6 as outlined below. The difference between the solutions of the two different meshes can be calculated by Equation (14):

$$\varepsilon_{21} = \varphi_2 - \varphi_1 \qquad \varepsilon_{32} = \varphi_3 - \varphi_2 \tag{14}$$

In this equations φ_1 denotes the solution of fine mesh or time step size, φ_2 denotes the solution of medium mesh or time step size and lastly φ_3 denotes the solution of coarse mesh or time step size. At this point, the convergence condition R can be calculated by Equation (15):

$$R = \frac{\varepsilon_{21}}{\varepsilon_{32}} \tag{15}$$

-1 < R < 0 Oscillatory convergence
0 < R < 1 Monotonic convergence
R < 1 Oscillatory divergence
R > 1 Monotonic divergence

The apparent order of p can be calculated by Equation (16):

$$p = \frac{\ln\left\|\varepsilon_{32}/\varepsilon_{21}\right| + q\right|}{\ln(r_{21})} \tag{16}$$

Here,

$$q = \ln\left(\frac{r_{21} - s}{r_{32} - s}\right) \tag{17}$$

$$s = \mathrm{sgn}(\varepsilon_{32}/\varepsilon_{21}) \tag{18}$$

are given as Equation (17) and Equation (18).

If the refinement factors (r_{21} and r_{32}) are the same, q is equal to zero. The extrapolated values are:

$$\varphi_{ext}^{21} = (r^p\varphi_1 - \varphi_2)/(r^p - 1) \tag{19}$$

The approximate relative error and extrapolated relative error are:

$$e_a^{21} = \left|\frac{\varphi_1 - \varphi_2}{\varphi_1}\right| \qquad e_{ext}^{21} = \left|\frac{\varphi_{ext}^{12} - \varphi_1}{\varphi_{ext}^{12}}\right| \tag{20}$$

At last, the GCI index can be calculated by:

$$GCI_{fine}^{21} = \frac{1.25e_a^{21}}{r_{21}^p - 1} \tag{21}$$

Numerical uncertainty originated from grid and time step size in the present study. Iteration uncertainty was neglected. The procedure states that when obtaining the uncertainty of one, the other must be kept constant. When grid uncertainty was performed, time step size was taken medium. On the other hand, for time step convergences, fine grid was used because grid convergence was reached. The numerical uncertainty for heave motion was given in Table 5a.

Table 5a: Numerical uncertainity for heave motion

	Grid Convergence	Time Step Convergence
φ_1	1.304	**1.360**
φ_2	1.286	1.297
φ_3	1.311	1.158
R	-0.720	0.450
GCI_{FINE}	4.89 %	4.72 %

Validation of Case no 6 was listed in Table 5b. In this table, CFD value was found for fine grid and fine time step size and experiment value was taken from the study of Irvine et al. (2008).

Table 5b: Validation of Case no 6.

Heave Motion TF	**CFD**	**Experiment**	**Difference**
	1.360	1.366	% 0.439

 ©2017: The Royal Institution of Naval Architects

5. RESULTS AND DISCUSSIONS

CFD calculations lasted approximately twelve hours on a 32-core processor with 128 GB RAM for thirty-second simulations for each case. This corresponds to a very short time period because the element number for the fine mesh was less than one million.

5.1 SHIP MOTIONS IN WAVES

The presented results and discussion on vertical motion calculations in regular head waves of DTMB 5512 in deep water are presented with figures and tables in this section. Ship motions in deep water were compared with experimental data of the same model (Irvine et al., 2008). Pitch and heave TF graphs for Fn=0.41 which were obtained by implementing CFD, strip theory and experiments are demonstrated in the figures.

In CFD simulations, time histories of the coupled pitch and heave motions were obtained using the fine grid φ_3 for all cases. As the first harmonics dominate the system for vertical motions of the whole frequency range, they were derived by implementing FS for each case. Then the TF's for vertical motions were generated and compared with the experimental data.

Figure 6 and Figure 7 reveal the non-dimensional pitch and heave amplitudes obtained by CFD, SMP and experimentally. The pitch response of the hull calculated by CFD is in excellent agreement with experiments over the entire frequency range as given in Figure 6. It may be said that the agreement of the strip theory results are comparatively poor. Over almost the entire frequency range, except for fe=1.4572, heave response CFD solutions were in very good accordance with experiments as can be seen from Figure 7. Generally, it can be said that CFD predictions were closer to the experiments. The results which are presented in Figure 6 and Figure 7 are tabulated in Table 6. Although the SMP result is also quite satisfactory, there are some differences when Table 6 is considered.

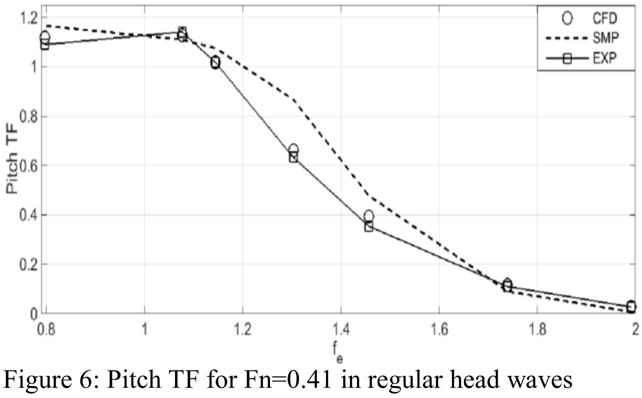

Figure 6: Pitch TF for Fn=0.41 in regular head waves

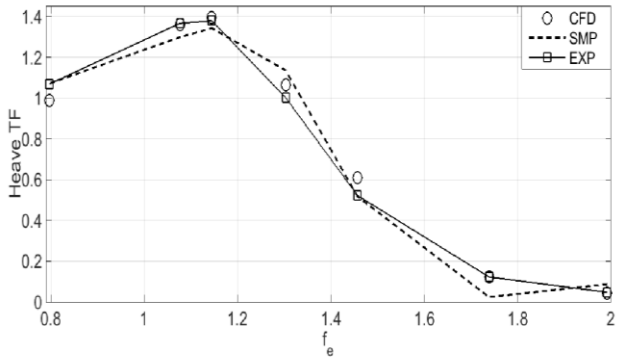

Figure 7: Heave TF for Fn=0.41 in regular head waves

Table 6: TF's for vertical motions

Case No.	Heave TF			Pitch TF		
	CFD	SMP	EXP.	CFD	SMP	EXP.
1	0.0436	0.087	0.0472	0.0276	0.007	0.0266
2	0.1250	0.024	0.1229	0.1166	0.091	0.1103
3	0.6108	0.517	0.5219	0.3923	0.478	0.3541
4	1.0631	1.136	1.0019	0.6619	0.867	0.6330
5	1.3958	1.343	1.3792	1.0196	1.075	1.0171
6	1.3601	1.298	1.3662	1.1287	1.110	1.1412
7	0.9890	1.072	1.0687	1.1172	1.166	1.0898

As mentioned earlier, the Fn=0.41 case is assumed to represent the high speed regime for a displacement vessel. In this case, the motions in waves flowing around the ship are highly turbulent and viscous effects are playing an important role. It is the main reason that at this speed nonlinear modelling returns better results compared to the linear strip theory. Besides, the complexity of the bulbous bow form and transom stern leads to generation of the flow separation phenomena which can only be calculated by a viscous solver. At the same time, in strip theory, hydrodynamic pressure is calculated by the first order velocity potential component. The second order velocity component is neglected. This assumption may lose its validity for relatively high speeds and should be reconsidered. In addition to these, excitation wave force is associated with simple sinusoidal form in potential strip theory. In real seaway, no wave has sinusoidal form due to gravitational force. However, in CFD analyses, a fifth order Stokes wave which is assumed to be more similar to the one generated from a wave generator is used. Finally, the Kelvin wave system of the ship at Fn=0.41 affects the ship motions in waves because the radiated waves from the ship have high amplitudes for transverse and divergent waves. This effect is included in CFD analyses. Therefore, it is strongly recommended that the reliable non-linear CFD tool should be used for high speed cases.

5.2 SHIP RESISTANCE IN WAVES

Before calculating added resistance in waves, the total resistance R_T must be obtained in calm water. R_T can be decomposed into two essential components - R_R (residuary resistance) and R_F (frictional resistance) as given in Equation (22):

$$R_T = R_R + R_F \tag{22}$$

Resistance is usually given in non-dimensional form as in Equation (23):

$$C_X = \frac{R_X}{\frac{1}{2}\rho S V^2} \tag{23}$$

where x in the subscript represents any resistance component. Here, ρ denotes the water density, S the wetted surface area and V the ship velocity. R_R and R_F are functions of Froude (Fn) and Reynolds (Re) numbers. The following statement can be expressed in Equation (24):

$$C_T = C_R(Fn) + C_F(Re) \tag{24}$$

Here, C_T denotes the total resistance coefficient, C_R the residuary resistance coefficient and C_F the frictional resistance coefficient. In the CFD calculation, the zeroth harmonic of the total resistance signal gives the averaged value of the predicted total resistance. Hence, the C_T of DTMB 5512 in calm water is achieved by implementing FS to the time series of the total resistance signal. The wave pattern of the ship at Fn=0.41 for the calm water case is given in Figure 8.

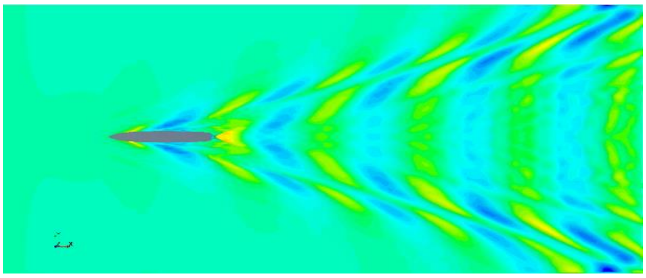

Figure 8: Presentation of the correctly captured Kelvin wave pattern behind the ship

As shown in Table 8, C_T is predicted with a high level of accuracy. The present study under-predicts C_T less than 0.5% as compared with the experimental data (Gui, 2001).

Table 8: Experimentally and numerically calculated total resistance coefficients

Calm Water Resistance	CFD	Experiment
	6.725 E-03	6.732 E-03

The added resistance in regular waves is calculated by using Equation (25):

$$C_{AW} = \frac{R_{AW}}{A^2 \rho g B^2 / L_{WL}} \tag{25}$$

Here, C_{AW} denotes the added resistance coefficient, A denotes the regular wave amplitude. B denotes the beam of the ship and L_{WL} denotes the water line length of the ship. In this equation, R_{AW} represents the added resistance value and it can be found by subtracting the calm water resistance R_T from the total resistance value for all cases. TF added resistance graphs are generated for all encountered frequencies except for Cases no. 1 and 2 as can be seen from Figure 9 because these two cases have two essential harmonic components when Fourier transform is applied to the total resistance signal as can be understood from Figure 10.

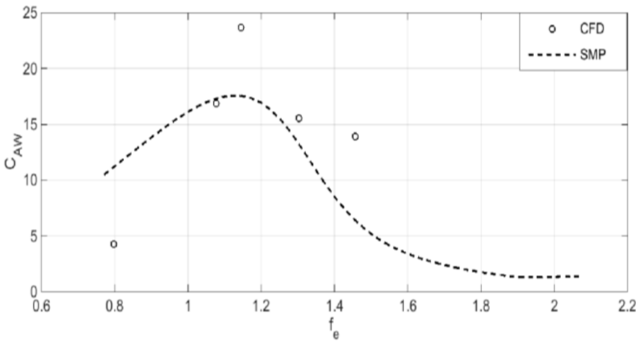

Figure 9: Added resistance TF for Fn=0.41

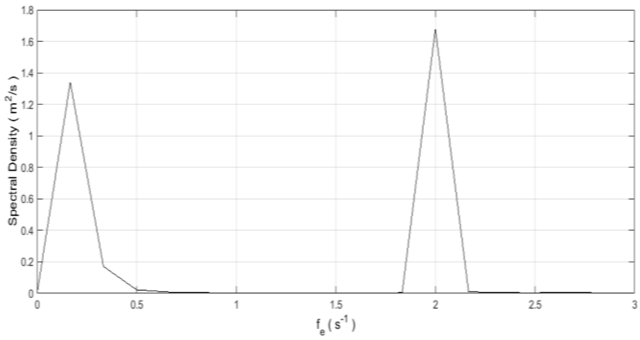

Figure 10: FFT analysis of total resistance signal for Case No. 1

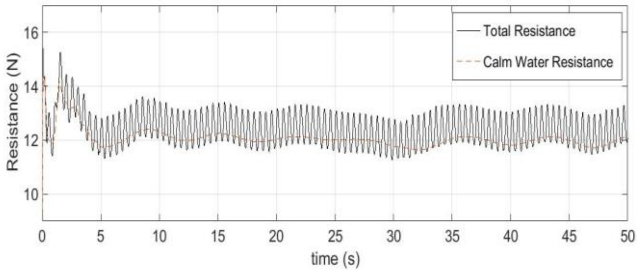

Figure 11: Computed time history of total resistance for Case No. 1 and calm water case

©2017: The Royal Institution of Naval Architects

As shown in Figure 11, the total resistance signal in waves does not oscillate around a fixed line which means the zeroth harmonic of the oscillation is time-dependent. This is the reason the average of the signal is not constant. Thus, the TF approach does not make any sense for these two frequencies and is excluded.

As commonly known, added resistance computation is second order with respect to the wave amplitude of incident waves based on computed motions. Referring to the study of Salvesen (1978), if one evaluates the vertical motions with an accuracy of around 10–15% then the resulting added resistance computations will likely to have an accuracy of around 20–30%. Due to this fact, the discrepancy of the computed vertical motions by utilizing CFD and SMP will cause a remarkable deviation on the added resistance outputs to appear. Moreover, it is known that Salvesen's method is based on calculating the second-order longitudinal wave force acting on the constant wetted surface of the vessel which has no viscosity effect at all. However, CFD tools enable fully non-linear governing equations to be solved by taking into consideration both the viscous effects and the draught change due to ship motions.

Added resistance in waves has become more insightful due to its direct relation with the EEDI (Energy Efficiency Design Index) which is mandatory for the construction of new ships, which significantly influences the CO2 amount emitted (IMO 2011, Seong-Oh Kim et al., 2014). Therefore, accurate calculation of the added resistance is needed to save the environment and to mitigate global warming to some level.

6. CONCLUSIONS

In the present paper, a promising approach to the problem of a fast displacement ship form, DTMB 5512, free to pitch and heave motions and added resistance in regular head waves was presented based on the numerical analyses using the URANS approach. The verification and validation studies were performed for the heave motion near-resonant case. The obtained results were compared with the corresponding outputs offered by the experiment and strip theory calculations where very good agreement was achieved for vertical motions in waves by using URANS. Added resistance calculations were only compared with respect to the strip theory because of the lack of experimental data. Remarkable differences between strip theory and URANS were observed on generated added resistance TF graphs. Therefore, the authors suggest that the URANS computed added resistance results reported here need a validation study.

7. ACKNOWLEDGMENT

This research was supported by Yildiz Technical University Scientific Research Projects Coordination Department. Project No: 2015-10-01-KAP01. The first author was supported by ASELSAN Graduate Scholarship for Turkish Academicians.

8. REFERENCES

1. BERTRAM V. *Practical Ship Hydrodynamics*. Butterworth-Heinemann. 2000
2. TEZDOGAN T., DEMIREL Y.K., KELLETT P., KHORASANCHI M., INCECIK A. and TURAN O. *Full-scale unsteady RANS CFD simulations of ship behavior and performance in head seas due to slow steaming*. Ocean Engineering, 186-206. 2015
3. SATO, Y., MIYATA, H. and SATO, T. *CFD simulation of 3-dimensional motion of a ship in waves: application to an advancing ship in regular heading waves*. Journal of Marine Science and Technology, 4: 108-116. 1999.
4. BECK, R.F. and REED, A.M. *Modern computational methods for ships in a seaway*. Transactions of the Society of Naval Architects and Marine Engineers, 109 pp.1-51.2001.
5. CARRICA, P.M,. WILSON, R. V. and STERN, F. *Unsteady RANS simulation of the ship forward speed diffraction problem*. Computers & Fluids 35 545–570. 2006.
6. CARRICA, P.M,. WILSON, R. V, NOACK, R. W., and STERN, F. *Ship motions using single-phase level set with dynamic overset grids*. Computers & Fluids 36 1415–1433. 2007
7. IRVINE, M., LONGO, J. and STERN, F., *Pitch and Heave Tests and Uncertainty Assessment for a Surface Combatant in Regular Head Waves*. Journal Ship Research, Vol. 52, No. 2, pp. 146-163. 2008.
8. WEYMOUTH, G.D., WILSON, R.V. and STERN, F. *RANS Computational fluid dynamics predictions of pitch and heave motion in head seas*. Journal of Ship Research. 49 (2): 80-97. 2005.
9. DENG, G.B., QUEUTEY, P. and VISONNEAU, M. *Seakeeping prediction for a container ship with RANS computation*. 22nd Chinese conference in hydrodynamics. 2009.
10. WILSON, R.V., JI, L., KARMAN, S.L., HYAMS, D.G., SREENIVAS, K., TAYLOR, L.K. and WHITFIELD, D.L. *Simulation of large amplitude ship motions for prediction of fluid-structure interaction*. 27th Symposium on Naval Hydrodynamics. Seoul. 2008.
11. QUERARD, A.B.G., TEMAREL, P. and TURNOCK, S.R. *The hydrodynamics of ship-like sections in heave, sway and roll motions predicted using an unsteady Reynolds averaged Navier-Stokes method*. Engineering for the Maritime Environment, 233. 2009.
12. BHUSHAN, S., XING, T., CARRICA, P. and STERN, F. Model and full-scale URANS simulations of Athena resistance, powering,

seakeeping, and 5415 manoeuvring. Journal of Ship Research, 53 (4), pp.179-198. 2009.

13. SIMONSEN, C.D., OTZEN, J.F., JONCQUEZ, S. and STERN, F. *EFD and CFD for KCS heaving and pitching in regular head waves*. Journal of Marine Science and Technology, 18 (4), pp.435-459. 2013.
14. SIMONSEN, C.D. and STERN, F. *CFD simulation of KCS sailing in regular head waves*. Gothenburg 2010-A Workshop on Numerical Ship Hydrodynamics. Gothenburg. 2010.
15. GUO, B.J., STEEN, S. and DENG, G.B. *Seakeeping prediction of KVLCC2 in head waves with RANS*. Applied Ocean Research, 35: 56-57. (4), pp.179-198. 2012.
16. OZDEMIR, Y.H. and BARLAS, B. *Numerical study of ship motions and added resistance in regular incident waves of KVLCC2 model*. International Journal of Naval Architecture and Ocean Engineering, 9:2, pp 149-159. 2017.
17. QUERARD, A.B.G., TEMAREL, P. and TURNOCK, S.R. *Influence of viscous effects on the hydrodynamics of ship-like sections undergoing symmetric and anti- symmetric motions, using RANS*. In: Proceedings of the ASME27th International Conference on Offshore Mechanics and Arctic Engineering (OMAE), Estoril, Portugal, pp.1–10. 2008.
18. CD-ADAPCO. *User guide STAR-CCM Version 9.0.2*. 2014.
19. INTERNATIONAL TOWING TANK CONFERENCE (ITTC), (2011b). *Practical guidelines for ship CFD applications*. In Proceedings of the 26th ITTC. 2011.
20. ROACHE, P. J., *Verification of Codes and Calculations*. AIAA J., vol. 36, no. 5, pp. 696–702, 1998.
21. CELIK, I., GHIA, U., ROACHE, P., FRETIAS, C.J. , COLEMAN, H., RAAD, P.E., *Procedure for estimation and reporting of uncertainty due to discretization in CFD applications*. J. Fluids Eng.-Trans. ASME, vol. 130, no. 7, Jul. 2008.
22. GUI, L., LONGO, J., and STERN, F. *Towing Tank PIV Measurement System, Data and Uncertainty Assessment for DTMB Model 5512*. Experiments in Fluids, Vol. 31, pp. 336-346. 2001.
23. FENTON, J. D. *A fifth-order Stokes theory for steady waves*, J. Waterw. Port. Coast. Ocean Engineering, 111 (2), 216-234. 1985.
24. KIM, S.O., OCK, Y.B., HEO, J.K., PARK, J.C., SHIN, H.S., LEE, S.K, *CFD simulation of added resistance of ships in head sea for estimating energy efficiency design index*, https://doi.org/10.1109/ Oceans-Taipei. 2014. 6964578, 07-10.04.2014.
25. SALVESEN, N., *Added Resistance of Ships in Waves*, Journal of Hydronautics, Vol. 12, No.1 (1978), pp. 24-34. http://dx.doi.org/10.2514/3.63110
26. CHOI, J., and SUNG, B. Y., *Numerical simulations using momentum source wave-maker applied to RANS equation model*, Coastal Engineering, 56 (10), pp. 1043 - 1060. 2009

 ©2017: The Royal Institution of Naval Architects